Supporting Information

Near 100% selectivity for ammonia synthesis at high current density by promoting nitrate protonation on copper dispersed todorokite-type manganese oxide

Shijia Li[a], Chuqian Xiao[a], Rongzhen Chen[a], Yuting Ma[a], Kaiwen Luo[a], Mengyi Wang[a], Muyao Shen[a], Yihua Zhu[a], Yuhang Li[a,*], and Chunzhong Li[a,b,*]

[a] *Key Laboratory for Ultrafine Materials of Ministry of Education, Shanghai Engineering Research Center of Hierarchical Nanomaterials, Frontiers Science Center for Materiobiology and Dynamic Chemistry, School of Materials Science and Engineering, East China University of Science & Technology, Shanghai 200237, China.*

[b] *School of Chemical Engineering, East China University of Science & Technology, Shanghai 200237, China.*

**E-mail: yuhangli@ecust.edu.cn; czli@ecust.edu.cn*

Table of Contents

Experimental Procedures

Chemicals and materials. Reagents for catalyst synthesis and characterization NaOH (Macklin), $KMnO_4$ (aladdin), $MnCl_2$ (aladdin), $Mg(CH_3COO)_2$ (aladdin), $Cu(NO_3)_2•6H_2O$ (aladdin), $Ni(NO_3)_2•6H_2O$ (aladdin), $Co(NO_3)_2•6H_2O$ (aladdin), Na_2SO_4 (aladdin), KNO_3 (Macklin), $Na^{15}NO_3$ (aladdin) and Nafion solution(Alfa Aesar China) were used as-received.

Catalyst preparation. Todorokite-type MnO_2 was obtained by autoclaving layer-structured MnO_2 (i.e. birnessite), which was synthesized by reactions of MnO_4^- and Mn^{2+} under strong alkaline conditions as reported in literature.[1] The preparation procedures are as follows.

Preparation of OMS-1. First, $Mn(OH)_2$ sol was obtained by adding 12.5 mL of 5 M NaOH solution into 10 mL of 0.5 M $MnCl_2$ solution under vigorous stirring. Then 10 mL of 0.2 M $KMnO_4$ solution was added dropwise into the above mixture under vigorous stirring and dark precipitates were formed. The MnO_4^-/Mn^{2+} mole ratio was set at 0.4. This suspension was aged at room temperature for 2 days, then centrifuged and washed with deionized water for 3 times. In order to fully remove the residual Cl^-, the solid was further dissolved in 50ml deionized water and stirred for 2 days then washed with deionized water and centrifuged to collect the sample. The layered phase thus obtained (Na-birnessite). Then, wet Na-birnessite sample was transferred into 50 mL of 1 M $Mg(CH_3COO)_2$ solution and stirred for 12 h for ion exchange of sodium ion with magnesium ion. After washed with deionized water for 3 times, the ion-exchanged sample was kept in the Teflon-lined autoclave at 140 ℃ for 24 h to form tunnel structure. The resultant solid product was filtered, washed with deionized water for 3 times and dried at 100 ℃ in an oven overnight. The obtained powder was ground and was denoted as OMS-1.

Preparation of Cu(x)-OMS-1. For copper modification, $Cu(NO_3)_2•6H_2O$ and $MnCl_2$ were simultaneously added into 10 mL of deionized water from the beginning of the above preparation

procedure. The subsequent steps were the same as those of the pure OMS-1. Four nominal Cu/Mn atomic ratios of, 0.1, 0.2, 0.3, 0.4, 0.8 and 2 in the starting mixture were chosen. For convenience, the Cu-modified OMS-1 samples were denoted as Cu(x)-OMS-1, where x represents the actual atomic ratio of Cu to Mn in the final product determined by inductively coupled plasmaoptical emission spectroscopy (ICP-OES, Vista-Mpx, Varian, USA), seeing Table S1.

Preparation of Ni-OMS-1. For nickel modification, $Ni(NO_3)_2 \bullet 6H_2O$ was added in the same ratio as Cu-OMS-1. The other steps were the same as those of Cu-OMS-1.

Preparation of Co-OMS-1. For cobalt modification, $Co(NO_3)_2 \bullet 6H_2O$ was added in the same ratio as Cu-OMS-1. The other steps were the same as those of Cu-OMS-1.

Characterization. The structures of the catalysts were observed by SEM (SU-8020) and TEM (FEI F30) equipped with anergy dispersive X-ray spectroscopy. The valence states of elements in the surface of catalysts were verified by XPS (ESCALAB 250Xi) and taking C 1s of 284.8 eV as internal reference. Inductively coupled plasma optical emission spectrometry (ICP-OES) was carried out on Agilent 720ES. X-ray powder diffraction (XRD) for powder analysis was carried out with a Ultima IV utilizing Cu Kα radiation (λ = 1.54178 Å). The Brunauer-Emmett-Teller (BET) surface areas were estimated over the relative pressure (P/P_0) range of 0.05–0.30. The pore size distribution was derived from the adsorption branch of the isotherms using the Barrett–Joyner–Halenda (BJH) model. Electron paramagnetic resonance (EPR) measurements were carried out on a Bruker EMXplus-6/1. The ultraviolet-visible (UV-Vis) absorbance spectra were measured on UV-2600 spectrometer. The isotope labeling experiments were measured by ^{1}HNMR measurement (Bruker 400-MHz system). Operando attenuated total reflection Fourier-transform infrared spectroscopy (ATR-FTIR) was performed on a iZ 10 FT-IR spectrometer. The Ge single crystal was used as the substrate for working electrode to ensure we can get enough IR signals. The adsorption capability and acidic active sites of the catalysts were assessed according to the temperature programmed desorption (TPD) curves of NH_3, which were acquired on a chemisorption

analyzer with a thermal conductivity detector (TCD) (Micrometrimetics AutoChem II 2920). Details of characterizing the solid phase with X-ray absorption fine structure (XAFS) analyses. Cu K-edge analysis was performed with Si(111) crystal monochromators at the BL11B beamlines at the Shanghai Synchrotron Radiation Facility (SSRF) (Shanghai, China). Before the analysis at the beamline, samples were pressed into thin sheets with 1 cm in diameter and sealed using Kapton tape film. The XAFS spectra were recorded at room temperature using a 4-channel Silicon Drift Detector (SDD) Bruker 5040. Cu K-edge extended X-ray absorption fine structure (EXAFS) spectra were recorded in transmission mode. Negligible changes in the line-shape and peak position of Cu K-edge XANES spectra were observed between two scans taken for a specific sample. The XAFS spectra of these standard samples (CuO and Cu foil) were recorded in transmission mode. Data reduction, data analysis, and EXAFS fitting were performed and analyzed with the Athena and Artemis programs of the Demeter data analysis packages[2] that utilizes the FEFF6 program[3] to fit the EXAFS data. The energy calibration of the sample was conducted through standard and Cu foil, which as a reference was simultaneously measured. A linear function was subtracted from the pre-edge region, then the edge jump was normalized using Athena software. The χ(k) data were isolated by subtracting a smooth, third-order polynomial approximating the absorption background of an isolated atom. The k^3-weighted $\chi(k)$ data were Fourier transformed after applying a HanFeng window function (Δk = 1.0). For EXAFS modeling, the global amplitude EXAFS (*CN, R,* σ^2 and ΔE_0) were obtained by nonlinear fitting, with least-squares refinement, of the EXAFS equation to the Fourier-transformed data in *R*-space, using Artemis software, EXAFS of the Cu foil are fitted and the obtained amplitude reduction factor S_0^2 value (0.849) was set in the EXAFS analysis to determine the coordination numbers (*CNs*) in the Cu-O and Cu-Mn scattering path in sample.

Electrochemical measurements. NITRR experiments were carried out in a H-cell separated by a Nafion 117 membrane in an electrochemical workstation (CHI 760E and DH7002). The cathode (i.e. the working electrode) was fabricated by spray-coating a catalyst ink (10 mg of catalyst powders and 40 μL of Nafion binder uniformly dispersed in 0.96 mL of ethanol) on a carbon paper. The reference electrode is Ag/AgCl

and platinum foil is the counter electrode. 30 mL mixed 0.5 M Na_2SO_4 (pH ≈ 6.84) / 0.05 M KNO_3 solution was the catholyte after purged by Ar and 30 mL pure 0.5 M Na_2SO_4 solution was anolyte. All potentials were calibrated to the reversible hydrogen electrode (RHE) reference by $E_{RHE} = E_{(V\ vs.\ Ag/AgCl)} + 0.0591*pH + 0.205$. j-V plots were performed with a scanning rate of 50 mV s^{-1} from −0.6 to −1.4 V vs. RHE. Chronoamperometry tests were carried out at different given potentials under continuous stirring. After the reaction for 2 hour, as-obtained cathodic electrolyte solution was collected for the following detection of different liquid products. Fresh electrolyte solutions were always used for each run. All the electrolytes were stored in the fridge. Cyclic voltammetry (CV) was managed at different sweep rates to test electrochemical double-layer capacitance (C_{dl}). Tafel slopes were determined according to the Tafel plots. The reaction order of the NO_3RR with respect to nitrate ions was estimated based on the slope of the fitting line of $\log(|J_{NH3}|)$ vs. $\log([NO_3^-])$. The apparent rate constant for the NO_3RR (k_{ap}) was obtained according to the pseudo-first order kinetic equation. Likewise, the equilibrium adsorption constant of NO_3^- on the catalyst surface (K_{ads}) could be assessed based on the linear expression of the Langmuir–Hinshelwood model, and thus the adsorption free energy could be calculated based on the thermodynamic formula. The apparent activation energy for NO_3RR (E_a)was determined according to the Arrhenius plot. Scan-rate-dependent LSV curves were measured to qualitatively analyze the reaction mechanism based on the relationship between the peak current density and the scan rate or the square root of the scan rate. Moreover, the charge transfer numbers of related reaction steps could be estimated according to the Nicholson–Shain equation. All equations are showed below:

Equation 1: Tafel plots

$E = a + b\log(J_{NH3})$, where E is the applied potential vs. RHE, J_{NH3} is the partial current density of NH_3, a is a constant and b is the Tafel slope.

Equation 2: Pseudo-first order kinetic equation

$\ln(C_0/C_t) = k_{ap}t$, where k_{ap} is the apparent rate constant, C_0 and C_t are the concentrations of NO_3^- in the electrolytes at the beginning and at reaction time t, respectively.

Equation 3: Linear expression of the Langmuir-Hinshelwood model

$1/r_0 = 1/(kK_{ads}C_0) + 1/k$, where K_{ads} is the equilibrium adsorption constants for NO_3^-, r_0 is the initial reduction rate of NO_3^- ($r_0 = k_{ap}C_0$), k is the rate constant for the adsorbed NO_3^-, C_0 is the initial concentration of NO_3^-.

Equation 4: Adsorption free energy of NO_3^-

$\Delta G_{ads} = -RTlnK_{ads}$ (16), whereΔG_{ads} is the adsorption free energy of NO_3^-, R is the gas constant, T is the reaction temperature and K_{ads} is the equilibrium adsorption constants for nitrate ions.

Equation 5: Apparent activation energy

$i_k = Ae^{(-Ea/RT)}$, where E_a is the apparent activation energy, i_k is the kinetic current at -0.5 V, A is the pre-exponential factor, T is the reaction temperature and R is the universal gas constant.

DFT Study. All the DFT calculations were conducted using the Dmol3 module of Materials Studios 2017.[4] The electronic exchange and related energy were treated using the Perdew, Burke and Ernzerhof (PBE) functional within the generalized gradient approximation (GGA).[5] The conductor like screening model (COSMO) method was adopted to consider the electrostatic interaction of adsorbate and water solvent.[6] The DFT semi-core pseudo potentials (DSPPs) core treatment with the relativistic effects were implemented to consider the core-electron (e^-) interaction, which superseded core e- by a single valid electricpotential to simplify the calculations.[7] The numerical basis set of double numerical plus polarization (DNP) was utilized. Thermal smearing of orbital occupation is set to 0.005 Ha (1 Ha = 27.21 eV). A 3×3×1 Monkhorst-Pack grid of special k-points was used for Brillouin zone integration. The SCF density convergence tolerance was 1×10^{-5} Ha. The maximum force, displacement, and energy of geometry optimal convergence tolerance are 0.004 Ha/Å, 0.005 Å, and 2×10^{-5} Ha. The standard hydrogen electrode (SHE) model was calculated the Gibbs free energy change (ΔG) for each basic step. Based on this method, the ΔG value can be determined as follows: $\Delta G = \Delta E + \Delta ZPE - T\Delta S + \int C_p dT$, where ΔE is the electronic energy difference calculated from DFT, ΔZPE is the change in zero-point energies, T is the ambient temperature, C_p is the heat capacity and ΔS is the entropy change. The thermodynamic properties of gas-phase molecules and ZPE contribution of adsorbed species are obtained through vibrational

frequencies. The computational hydrogen electrode (CHE) model was utilized to specify the Gibbs free energy of the proton-electron pair as the function of electrical potential.[8-9] We applied in this work the same free energy corrections for the gaseous species and solvation effect as in Refs.[10-11]

Determination of ion concentration. The ultraviolet-visible (UV-Vis) spectrophotometer was used to detect the ion concentration of pre-and post-test electrolytes after diluting to appropriate concentrations to match the range of calibration curves. The specific detection methods are as follows:

Determination of ammonia: The amount of NH_3 in the solution was determined by colorimetry using the indophenol blue method.[12] The reagents required for the indophenol blue method are potassium sodium tartrate-salicylic acid solution, sodium hypochlorite solution, and sodium nitrosoferricyanide solution. Potassium sodium tartratesalicylic acid solution was configured by weighing 50 g of salicylic acid [$C_6H_4(OH)COOH$], adding about 100 mL of deionized water, then adding 160 mL of 2 M sodium hydroxide solution, followed by stirring for complete dissolution; then 50 g of potassium sodium tartrate ($KNaC_4H_6O_6 \cdot 4H_2O$) was dissolved in water, and the above solution was combined into a 1000 mL volumetric flask and diluted with water to the standard line. Sodium hypochlorite solution was prepared by diluting with water and sodium hydroxide solution into sodium hypochlorite solution containing 3.5 g L^{-1} and 0.75 mol L^{-1} free base concentration. Sodium nitrosoferricyanide solution was prepared by weighing 0.1 g of sodium nitroso ferricyanide ($Na_2[Fe(CN)_5NO] \cdot 2H_2O$) into a 10 mL colorimetric tube and adding water to the standard line. The usual method for sample determination was to take 10 μL of the reacted solution and add 200 μL of sodium nitrosoferricyanide solution, 2 mL of sodium potassium tartrate solution-salicylic acid and 1 mL of sodium hypochlorite solution, followed by dilution with water to 10 mL. After color development for 120 min, the absorbance was then measured at 655 nm using a 10 mm cuvette with water as reference. A standard curve was established with a series of standard concentrations of ammonium chloride solution.

Determination of nitrite: The NO_2^- concentration was analyzed using the Griess test.[13] Grice's reagent was prepared by adding 250 mL of H_2O and 50 mL of phosphoric acid to a 500 mL beaker, adding 20.0

g of p-aminobenzene sulfonamide; then dissolving 1.00 g of N-(1-naphthyl)-ethylenediamine dihydrochloride in the above solution, transferring it to a 500 mL volumetric flask and diluting it with water to the mark. The general test method is: take 10 μL of the electrolyte after the reaction, add a certain amount of deionized water to dilute it, and subsequently add 1 mL of Gris reagent to mix well. After placing the mixed liquid at room temperature for 20 min, the absorbance was measured at the wavelength of 540 nm within 2 h using a cuvette with an optical range of 10 mm and water as a reference. Subsequently, the concentration of NO_2^- was calculated according to the concentration dilution times. Its standard curve was established by a series of standard concentrations of nitrite solution with the same test method.

Determination of nitrate: The NO_2^- concentration was analyzed using ion chromatography.

Determination of N_2H_4: The amount of possible N_2H_4 by-product in the electrolyte was determined using the Watt–Chrisp method.[14] The colour reagent was a mixture containing 0.5 g of p-dimethylaminobenzaldehyde, 25 mL of ethanol and 2.5 mL of concentrated HCl. Both the pristine blank electrolyte and the cathodic electrolyte were diluted 300 times using deionized water. Standard solutions of N2H4 in the diluted blank electrolyte (0.2, 0.4, 0.6, 0.8, 1.0 ppm) were prepared to build the calibration curve. Then, 0.1 mL of concentrated HCl solution was added to 4 mL of N_2H_4 standard solutions or diluted electrolytes to adjust the pH values of the solutions to the acidic range, followed by the addition of 0.5 mL of colour reagent. The resulting solutions were then allowed to stand for 5 min. Subsequently, UV-vis absorption spectra were measured in the wavelength range of 400–500 nm at a scan rate of 300 nm min−1. The maximum absorbance ought to occur at about 455 nm. According to the calibration curve and the measured absorbance, the concentration of N_2H_4 could be determined.

Isotope labeling experiments. 99 % $Na^{15}NO_3$ was used as the feeding N-source to perform the isotopic labeling nitrate reduction experiments, to clarify the source of ammonia. 0.5 M Na_2SO_4 was used as the electrolyte and $Na^{15}NO_3$ with a concentration of 0.05 M $^{15}NO_3^-$ (^{15}N) was added into the cathode chamber as the reactant. After electroreduction, electrolyte with obtained $^{15}NH_4^+$ (^{15}N) was taken out and the pH

value was adjusted to be weak acid with 1M H_2SO_4 for further quantification by ^1H NMR (400 MHz) with external standards of maleic acid.

Calculation of the yield and Faradaic efficiency.

For nitrate electroreduction, the yield was calculated by the Eq.1:

$$Yield_{NH3} = (c_{NH3} \times V) / (M_{NH3} \times t \times S) \quad (1)$$

The Faradaic efficiency was defined from the electric charge consumed for synthesizing ammonia and total charge passed through the electrode according to Eq. 2:

$$Faradaic\ efficiency = (8F \times c_{NH3} \times V) / (M_{NH3} \times Q) \quad (2)$$

The partial current density of NH_3 was calculated by the Eq.3:

$$J_{NH3} = J_{total} \times FE_{NH3} \quad (3)$$

Where,

c_{NH3} is the mass concentration of NH_3(aq);

V is the volume of electrolyte in the cathode compartment (30mL);

M_{NH3} is the molar mass of NH_3;

t is the electrolysis time (2 h);

S is the geometric area of working electrode (1 cm^2);

c is the generated concentration of ammonia or nitrite;

F is the Faradaic constant (96485 C mol^{-1});

Q is the total charge passing the electrode.

Results and Discussion

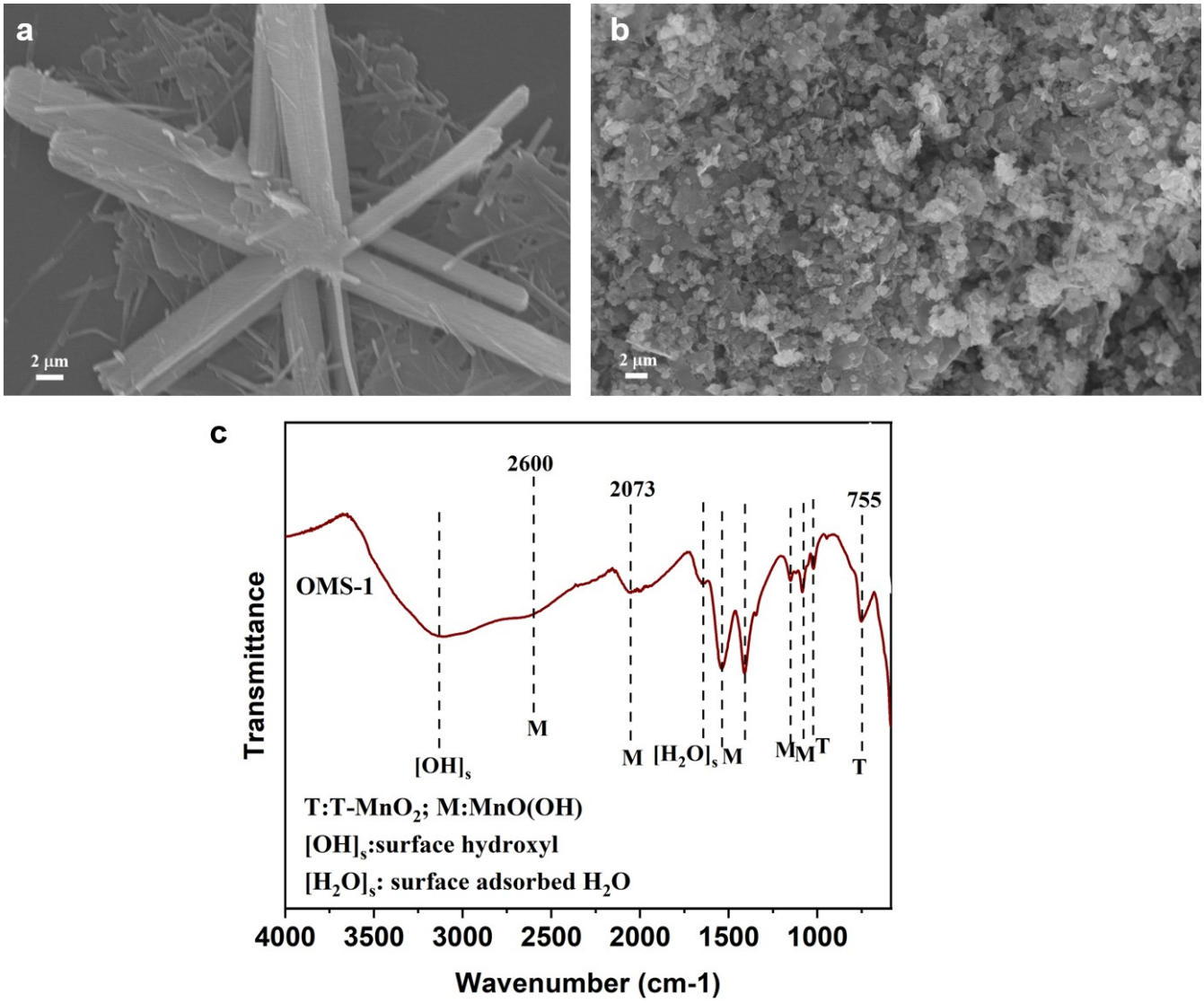

Figure S1. SEM images of (a) OMS-1 and (b) Cu(0.31)-OMS-1. (c) ATR spectra of OMS-1. The band at 755 cm^{-1} means the formation of tunnel structure[1,2].

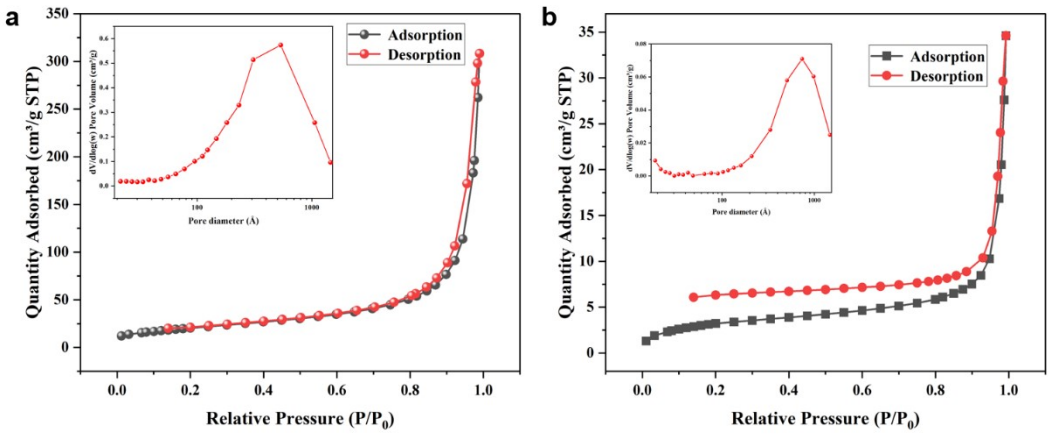

Figure S2. Nitrogen adsorption-desorption isotherms and BJH pore size distributions (inset) for (a) Cu(0.31)-OMS-1 and (b) OMS-1.

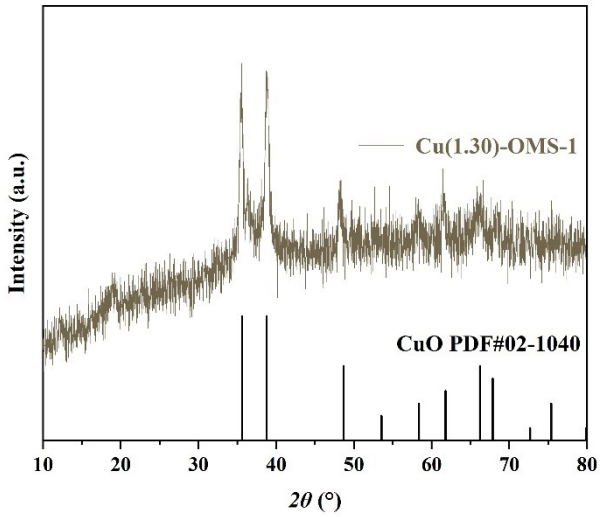

Figure S3. XRD pattern of Cu(1.30)-OMS-1.

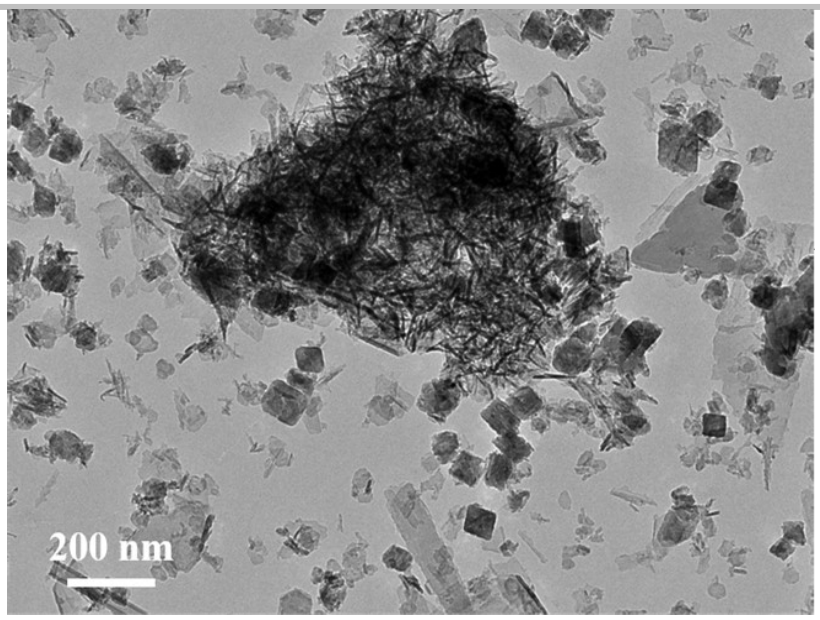

Figure S4. TEM image of Cu(0.31)-OMS-1

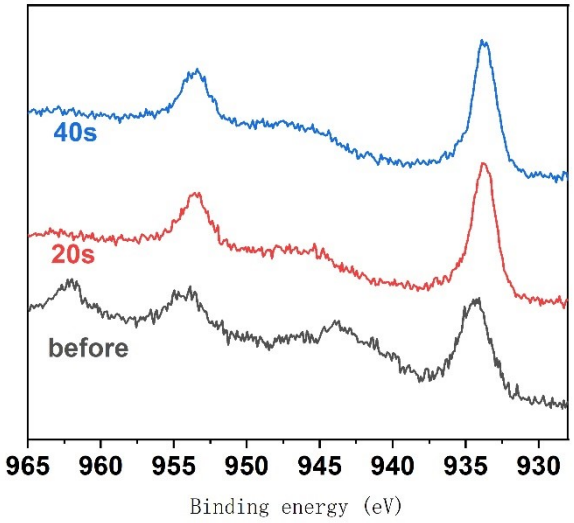

Figure S5 High-resolution depth-profiling XPS spectra of Cu 2p before and after 20 and 40s Ar ion bombardment, respectively.

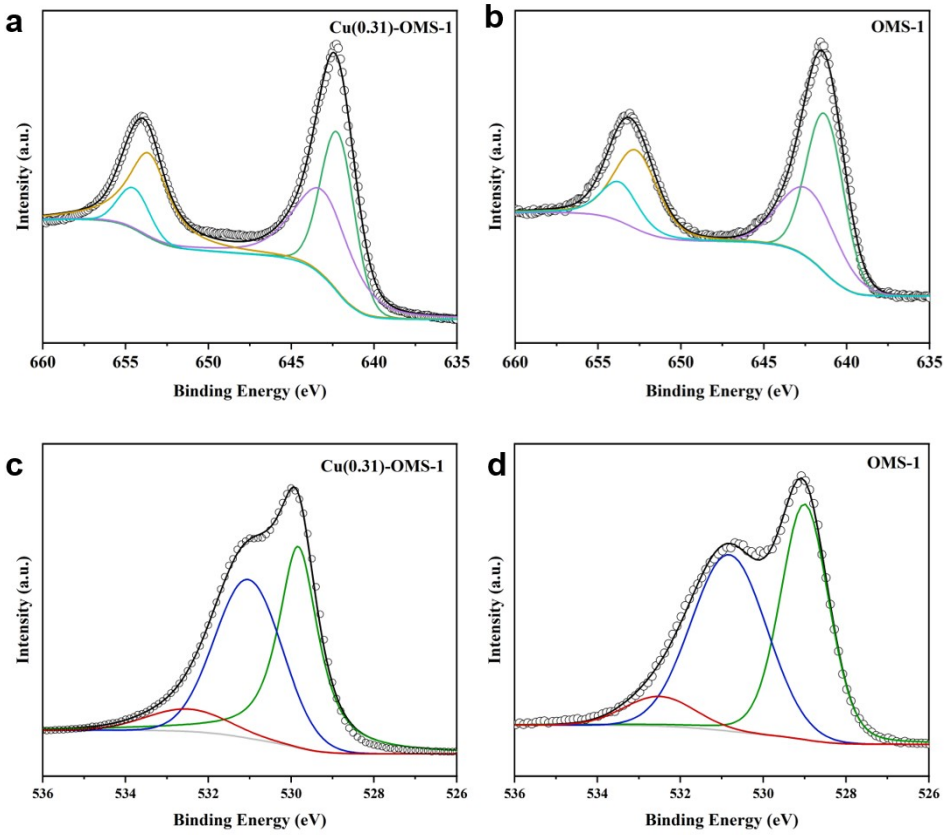

Figure S6. XPS Mn 2p (a, b) and O 1s (c, d) spectra of Cu(0.31)-OMS-1 and OMS-1.

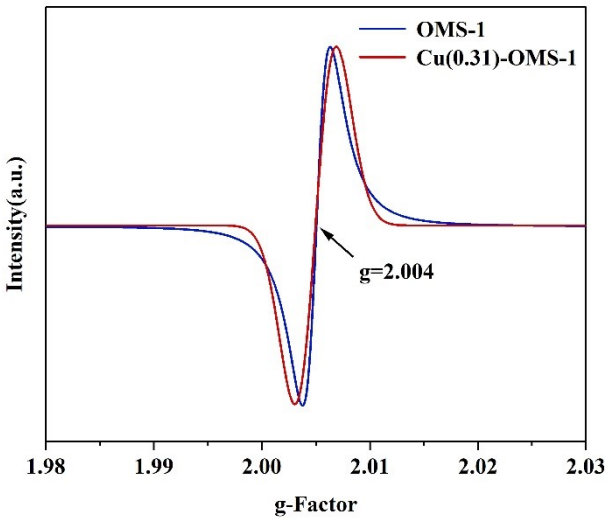

Figure S7. EPR characterization of Cu(0.31)-OMS-1 and OMS-1.

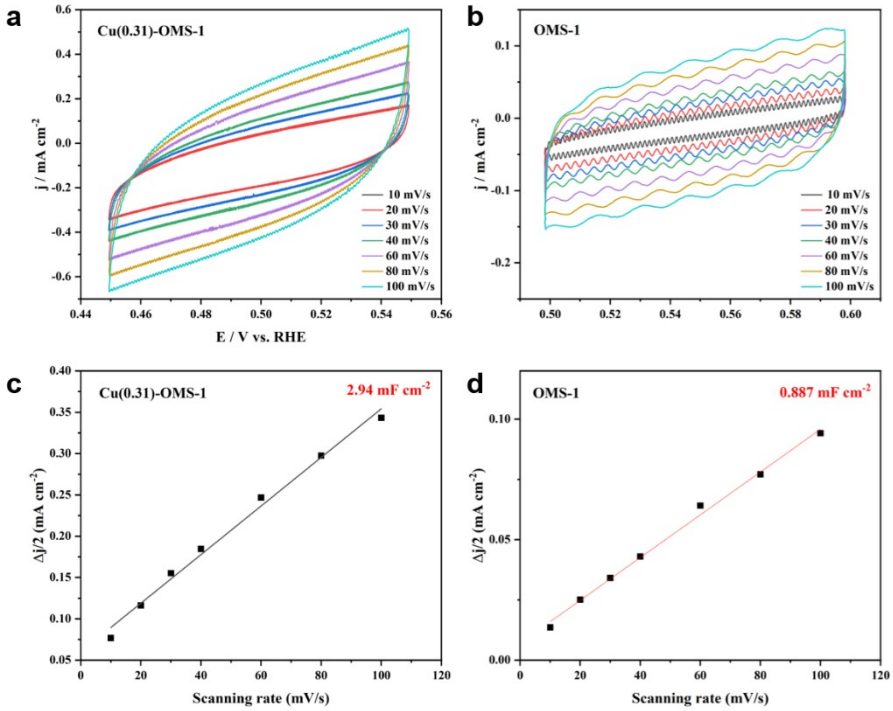

Figure S8. ECSA measurements of Cu(0.31)-OMS-1 and OMS-1 catalyst. (a, b) The cyclic voltammetry profiles obtained on the Cu(0.31)-OMS-1 and OMS-1 catalyst at the sweep rates of 10, 20, 30, 40, 60, 80, and 100 mV s^{-1}, respectively. (c, d) The determination of double layer capacitance for each catalyst.

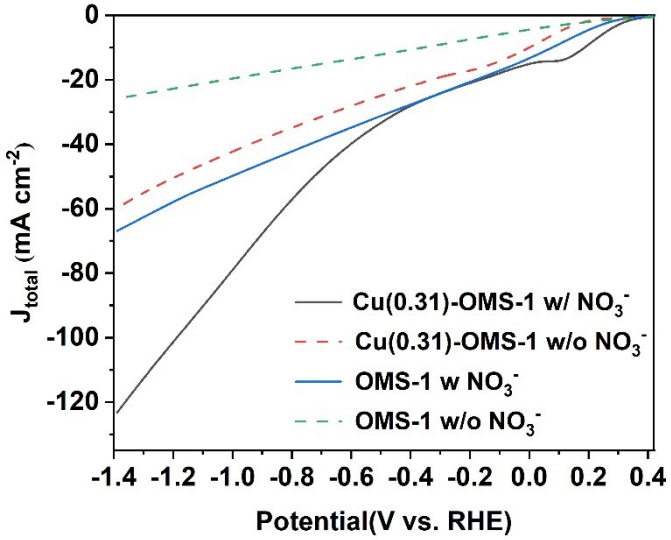

Figure S9. j−V plots were conducted with a scanning rate of 5 mV s^{-1} in 0.5 M Na_2SO_4 without or with various NO_3^- concentrations.

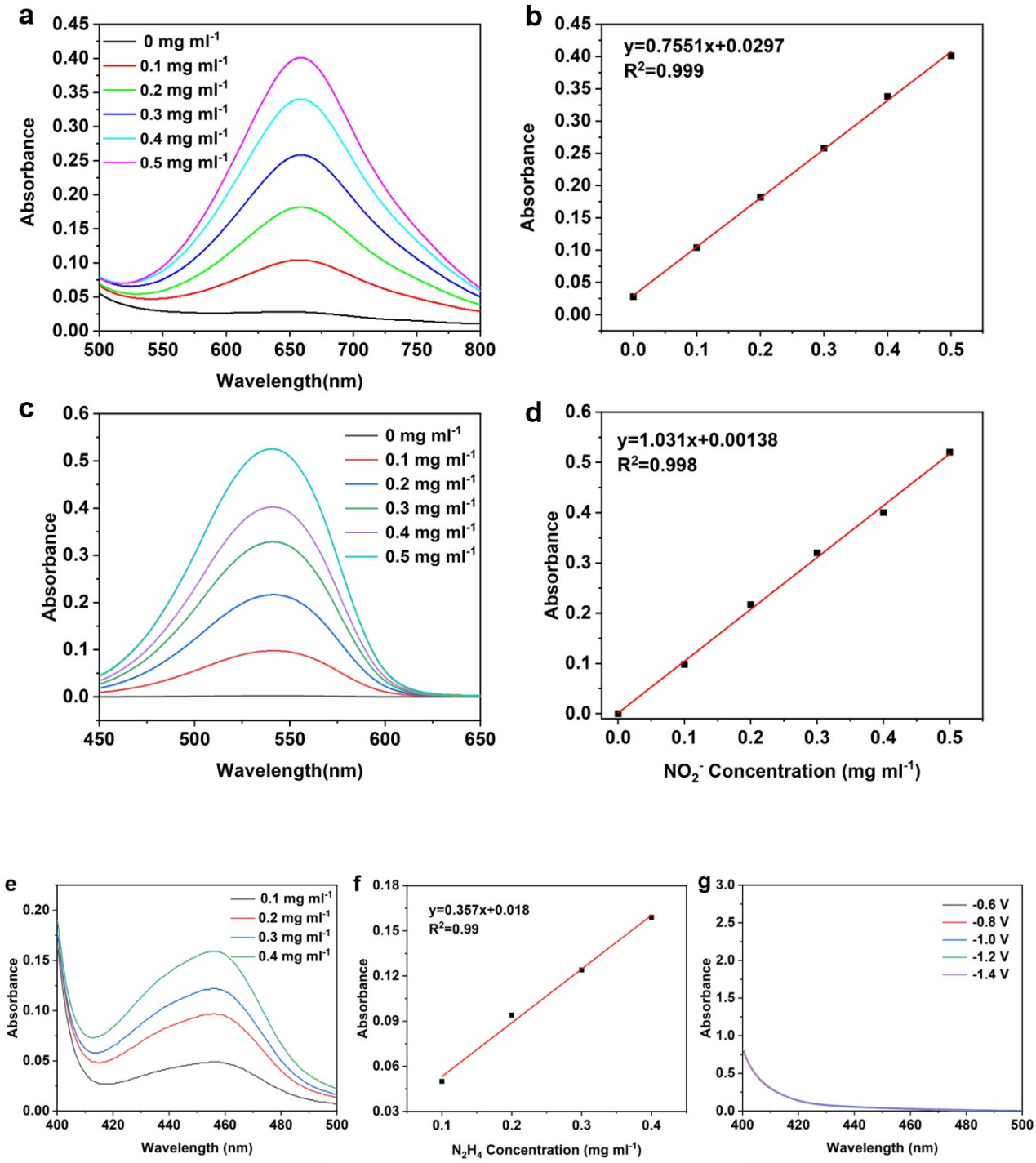

Figure S10. Ammonia detection using indophenol blue method. (a) The ultraviolet-visible adsorption spectra of different solution with different ammonia concentrations. (b) The linear standard curve for the calculation of ammonia production. Determination of the possible by-product of N_2H_4 using the Watt-Chrisp method. (a) UV-vis absorption spectra, (b) the calibration curve and (c) UV-vis absorption spectra of the catholytes with the addition of the color reagent after electrolysis at different potentials.

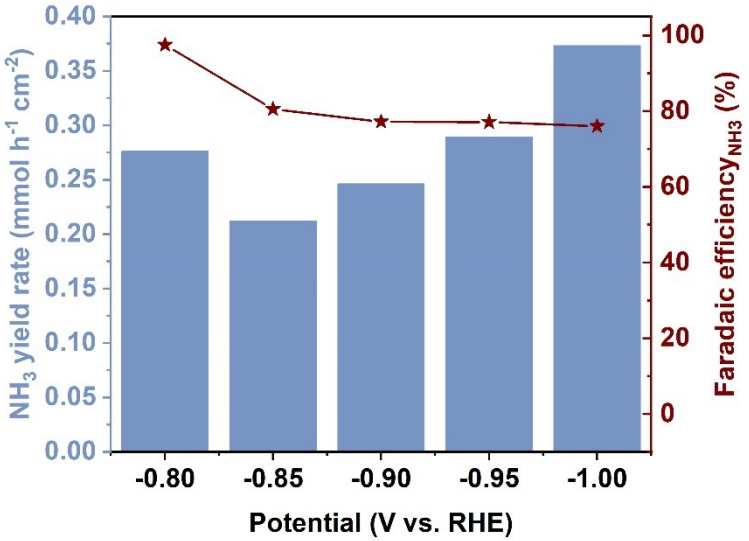

Figure S11 NH_3 yield rate and FE_{NH3} of Cu(0.31)-OMS-1 for reducing NO_2^- at various potentials.

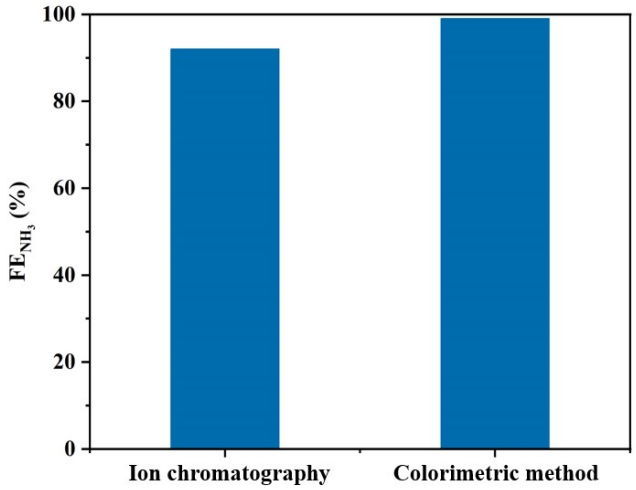

Figure S12. Comparison of colorimetric and ion chromatography quantitative results. The result showed the colorimetric results were very accurate.

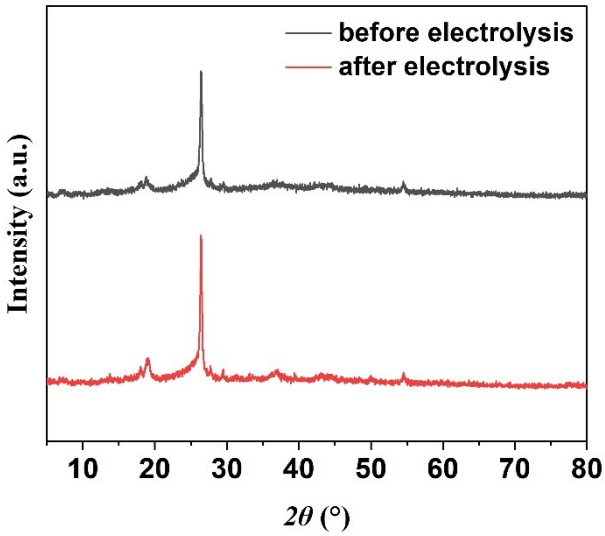

Figure S13. XRD patterns of Cu(0.31)-OMS-1 sprayed on carbon paper (before and after electrolysis).

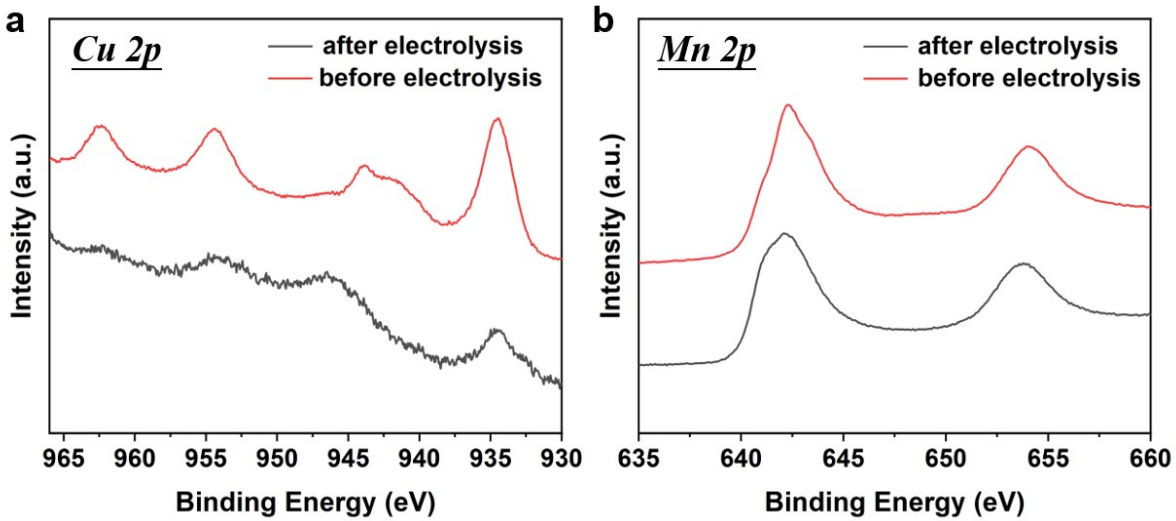

Figure S14. XPS spectra of Cu(0.31)-OMS-1 catalyst (before and after test). (a) Cu 2p XPS spectrum of Cu(0.31)-OMS-1 catalyst. (b) Mn 2p XPS spectrum of Cu(0.31)-OMS-1 catalyst.

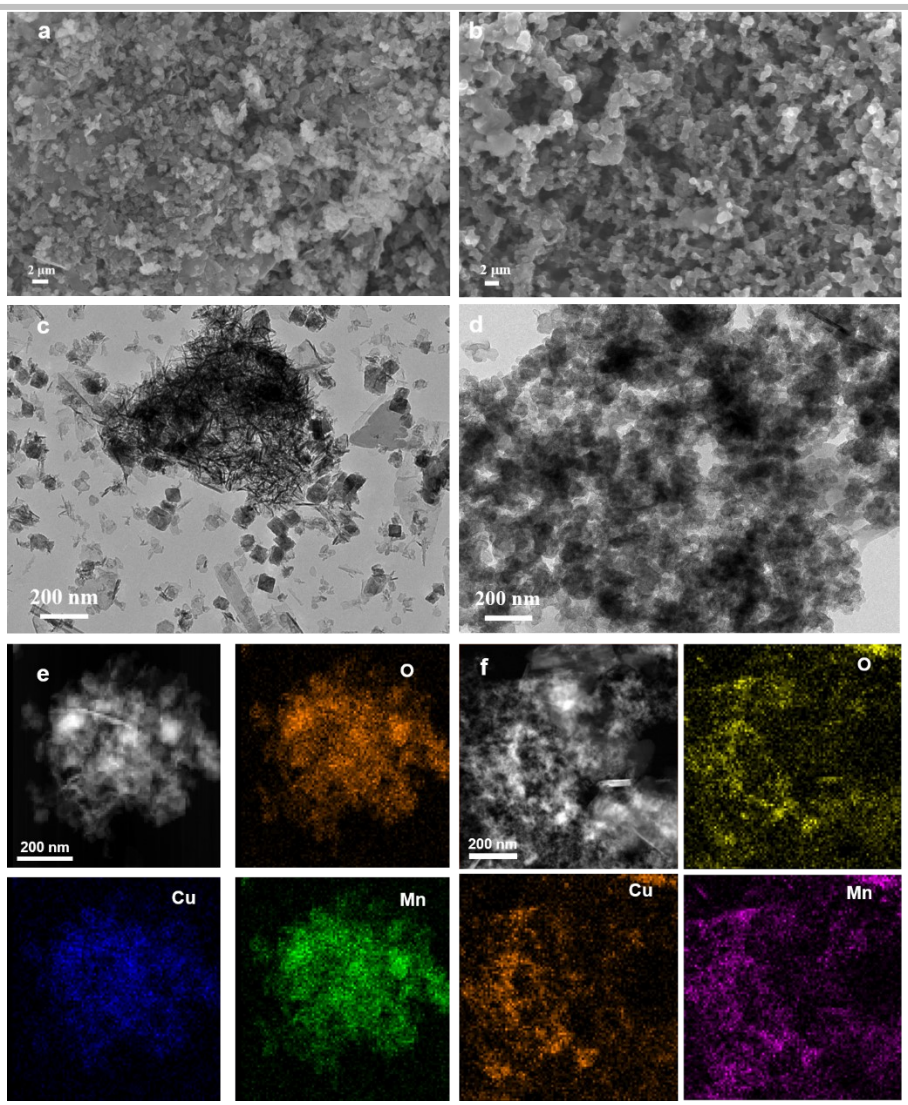

Figure S15 SEM (a), TEM (c) and HAADF-STEM (e) images of Cu(0.31)-OMS-1 catalyst before electrolysis. SEM (b), TEM (d) and HAADF-STEM (f) images of Cu(0.31)-OMS-1 catalyst after electrolysis.

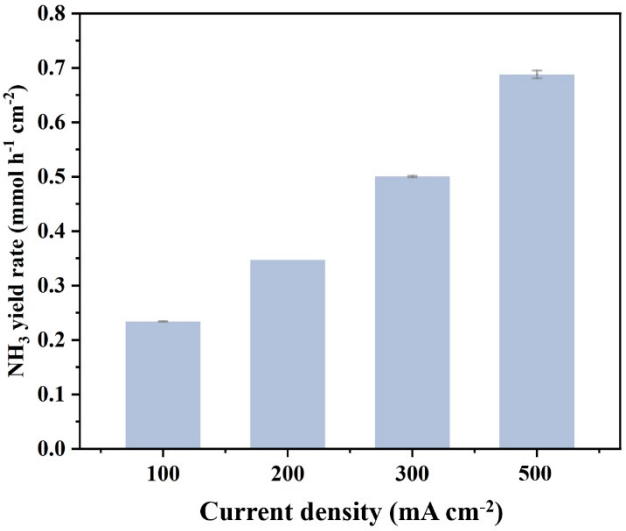

Figure S16. NH_3 yield rate of Cu(0.31)-OMS-1 at high current density in flow cell.

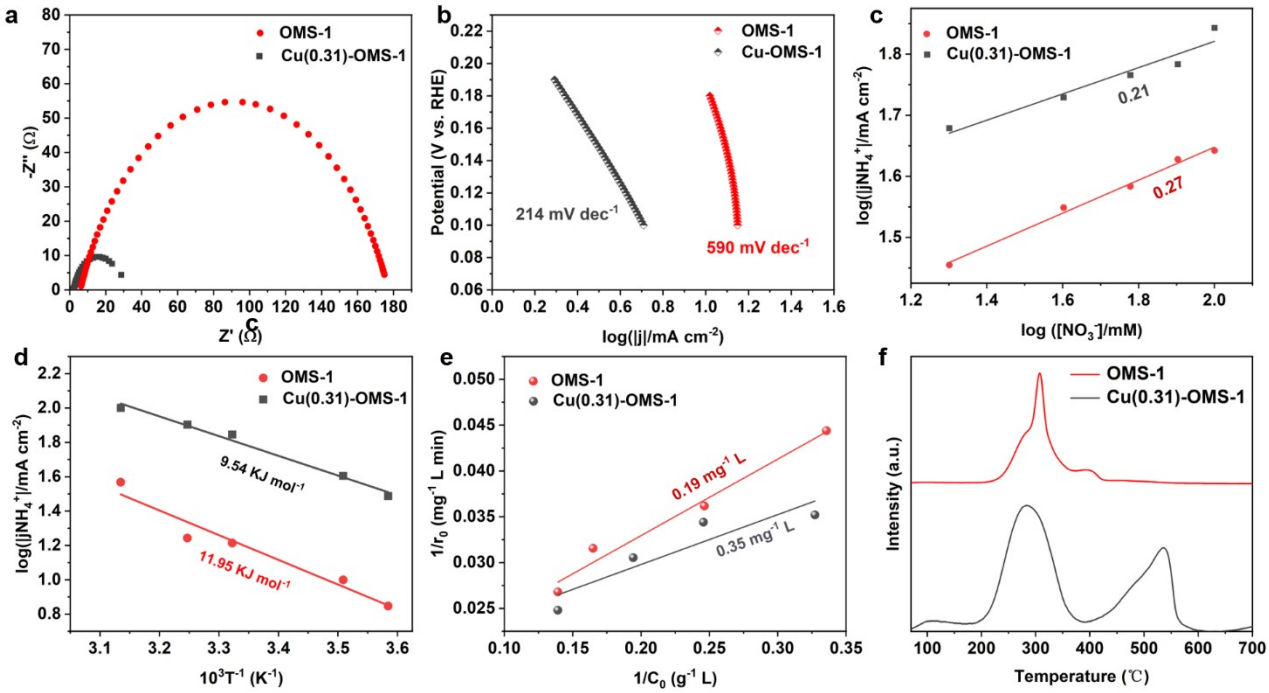

Figure S17 (a) Nyquist plots. (b) Tafel plots. (c) Reaction orders with respect to nitrate ions. (d) Apparent activation energies derived from Arrhenius plots. (e) Equilibrium adsorption constants of nitrate ions based on the Langmuir–Hinshelwood model. (f) NH3-TPD curves of Cu-OMS-1 and OMS-1

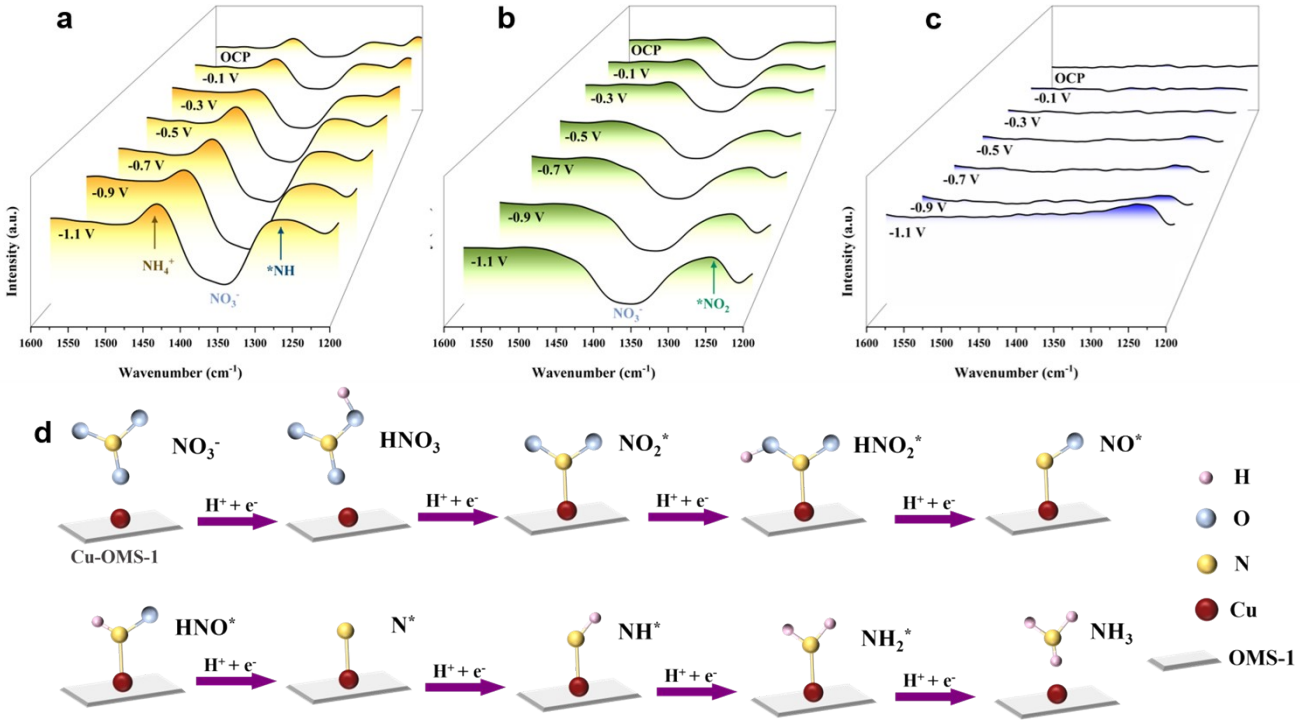

Figure S18. Potential-dependent operando FTIR spectra of (a) Cu(0.31)-OMS-1, (b) Cu(1.30)-OMS-1 and (c) Cu(0.10)-OMS-1 in Si single crystal during the NO_3RR electrolysis from OCP to −1.1 V vs. Ag/AgCl. (d) The simplified structures of various reaction intermediates along the reaction pathway of NITRR on the Cu(x)-OMS-1 model.

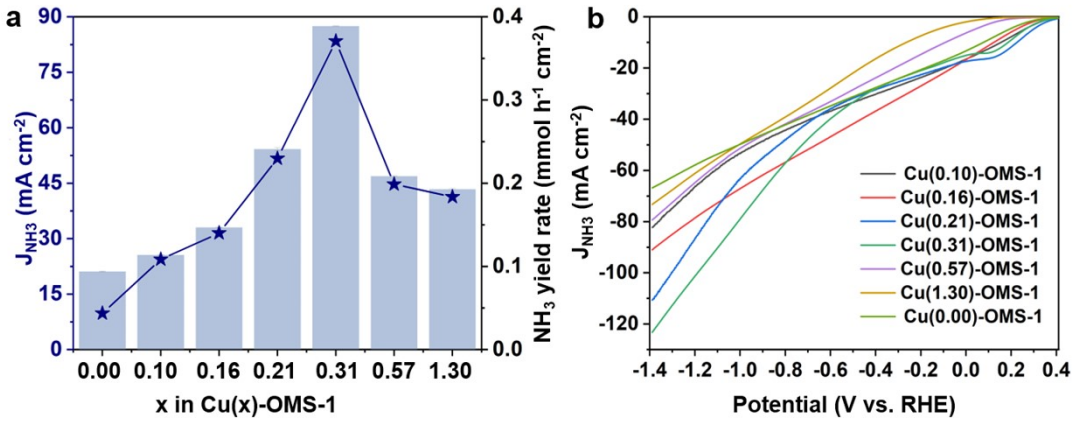

Figure S19. a) J_{NH3} and NH_3 yield rate of Cu(x)-OMS-1 at −1.0 V vs. RHE and b) j−V plots of NITRR on Cu(x)-OMS-1 in 0.5 M Na_2SO_4 + 0.05 M KNO_3 electrolyte.

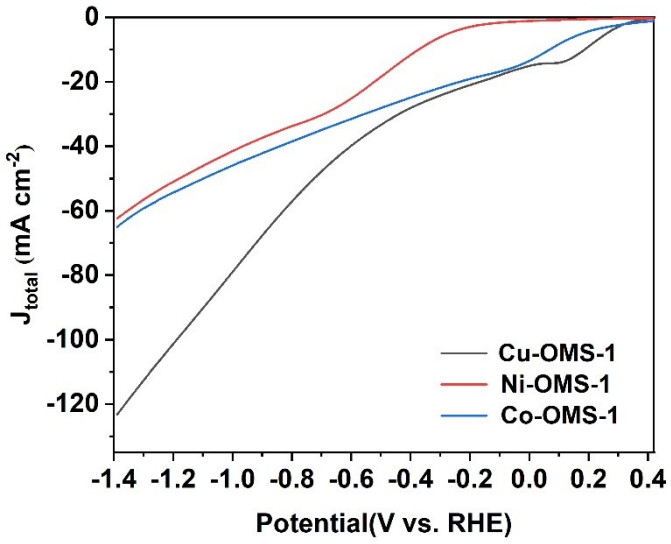

Figure S20. j−V plots of Cu-OMS-1, Co-OMS-1 and Ni-OMS-1 were conducted with a scanning rate of 50 mV s^{-1} in 0.5 M Na_2SO_4 with 0.05 M NO_3^-.

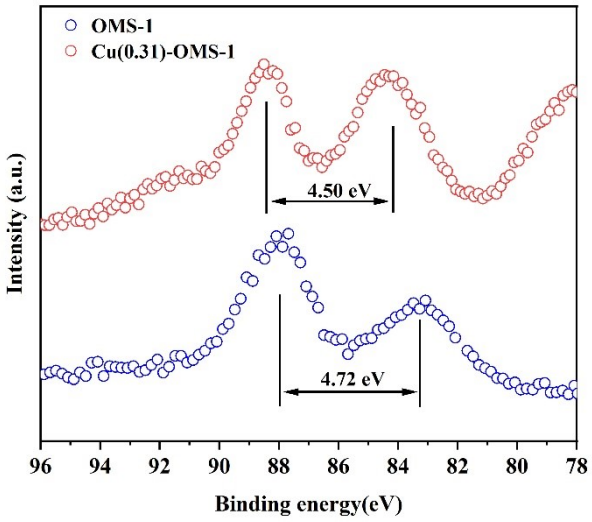

Figure S21. Mn 3s XPS spectrum of the as-prepared Cu(0.31)-OMS-1 and OMS-1 catalysts. The arrows indicate a shoulder peak.

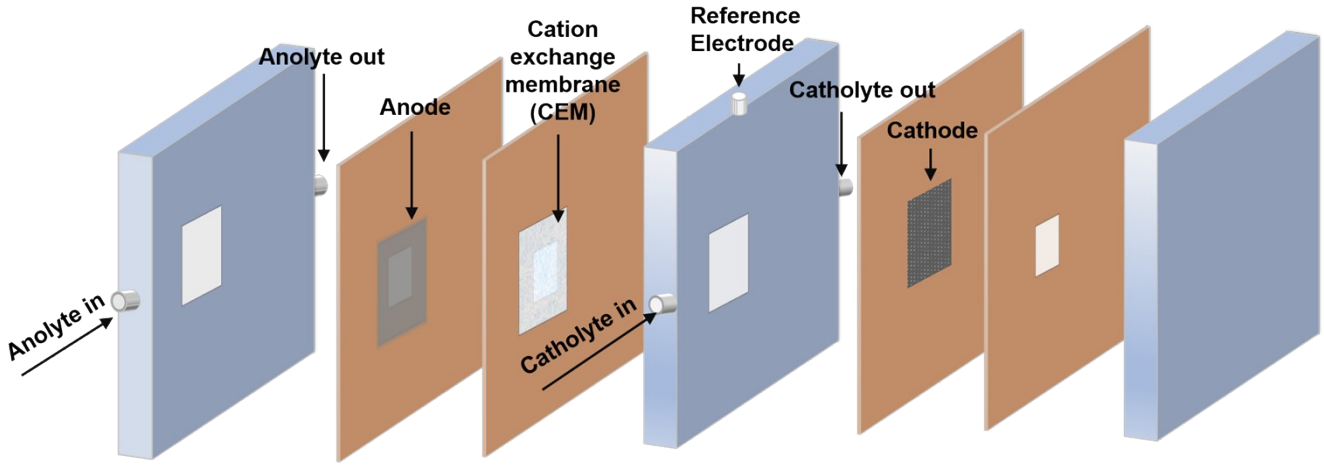

Figure S22. Schematic illustration of the flow-cell setup.

Table S1. Effect of the synthesis conditions on the formation of OMS-1[a] according to the ICP-OES results.

Sample notation	Element content(wt%)				Element content(mol/g)				Cu/Mn(mol/mol)
	Mn	Cu	K	Mg	Mn	Cu	K	Mg	
Cu(0.10)-OMS-1	59.56	6.80	0.08	0.43	1.08	0.11	0.00	0.02	0.10
Cu(0.16)-OMS-1	52.22	9.86	0.04	0.34	0.95	0.16	0.00	0.01	0.16
Cu(0.21)-OMS-1	47.22	11.26	0.1	0.69	0.86	0.18	0.00	0.03	0.21
Cu(0.31)-OMS-1	41.67	15.11	0.18	3.05	0.76	0.24	0.00	0.13	0.31
Cu(0.57)-OMS-1	32.86	21.85	0.27	2.48	0.60	0.34	0.00	0.10	0.57
Cu(1.30)-OMS-1	23.82	35.88	0.18	1.53	0.43	0.56	0.00	0.06	1.30

a Detailed synthesis conditions are described in the Experimental Section.

Table S2 EXAFS fitting parameters at the Cu K-edge for Cu-OMS-1, Cu-foil and CuO**.**

Sample	Shell	CN[a]	R(Å)[b]	σ^2(Å^2)[c]	ΔE_0(eV)[d]	R factor
Cu-foil	Cu-Cu	12*	2.540±0.003	0.0087±0.0003	3.8±0.4	0.0016
CuO	Cu-O	4.2±0.2	1.952±0.001	0.0052±0.0008	7.1±0.4	0.0048
	Cu-Cu	5.6±0.8	2.916±0.001	0.0085±0.0011	9.8±0.7	
	Cu-Cu	5.5±0.8	3.111±0.001			
Cu-OMS-1	Cu-O	3.7±0.2	1.955±0.001	0.0054±0.0008	4.4±0.3	0.0064
	Cu-Mn	0.8±0.3	2.903±0.001	0.0048±0.0029	-0.2±1.5	

[a]*CN*, coordination number; [b]*R*, the distance to the neighboring atom; [c]σ^2, the Mean Square Relative Displacement (MSRD); [d]ΔE_0, inner potential correction; *R* factor indicates the goodness of the fit. $S0^2$ was fixed to 0.849, according to the experimental EXAFS fit of Cu foil by fixing *CN* as the known crystallographic value. * This value was fixed during EXAFS fitting, based on the known structure of Cu.

Table S3. Binding energy and fraction of synthesized Cu(0.31)-OMS-1 and OMS-1 catalysts*.

Sample notation	Binding energy of O 1s (eV)			Binding energy of Mn $2p_{3/2}$ (eV)		AOS[b]
	Adsorbed molecular water	Adsorbed oxygen species	Lattice oxygen	Mn (III)	Mn (IV)	
OMS-1	532.5(7.50%)	530.82(47.74%)	529(44.74%)	641.3(59.54%)	642.3(40.45%)	3.71
Cu(0.31)-OMS-1	532.5(9.39%)	531(46.90%)	529.79(43.69%)	642.2(48.62%)	643.1(51.37%)	3.97

* Values in parentheses are peak percentages. [b] AOS: Surface average oxidation state. The values in parentheses were estimated by fitting the XPS spectra as multiplets according to the procedures in references 6 and 7.

Table S4. Comparing the NITRR activity of Cu(0.31)-OMS-1 in H-type cell with other reported effective electrocatalysts

Sample notation	Electrolyte	FE (%)	Partial current density (mA cm^{-2})	NH_3 yield rate (mmol h^{-1} cm^{-2})	Ref.
Cu(0.31)-OMS-1	**50 mM NO_3^- + 500 mM Na_2SO_4**	**99.7**	**108**	**0.51**	**This work**
Ru_1Cu_{10}/rGO	100 mM NO_3^- + 1000 mM KOH	98.0	~20	0.38	*Adv. Mater.*, ***2023**, 35, 2202952.*
a-RuO_2	200 ppm NO_3^- + 500 mM Na_2SO_4	97.5	~50	0.12	*Angew. Chem. Int. Ed.*, ***2022**, 61, e202202556.*
Meso-PdX NCs	5 mM NO_3^- + 100 mM Na_2SO_4	96.1	~35	0.05	*Adv. Mater.*, ***2023**, 35, 2207305.*
Cu/Cu_2O NW	200 ppm NO_3^- + 500 mM Na_2SO_4	95.8	~105	0.24	*Angew. Chem. Int. Ed.*, ***2020**, 59, 5350-5354.*
Cu-PTCDA	500 ppm NO_3^- + 100 mM PBS	85.9	~20	0.02	*Nat. Energy*, ***2020**, 5, 605-613.*
Cu SAG	20 mM NO_3^- + 100 mM PBS	~78.0	~8	0.03	*J. Am. Chem. Soc.*, ***2023**, 145, 6471-6479.*
SN Co-Li^+/PCNF	500 mM NO_3^- + 500 mM Na_2SO_4	72.7	~225	0.71	*Adv. Energy Mater.*, ***2022**, 12, 2202247.*
Fe SAC	500 mM NO_3^- + 500 mM K_2SO_4	69.0	35.3	0.46	*Nat. Commun.*, ***2021**, 12, 2870.*
CuCoSP	50 mM NO_3^- + 1000 mM KOH	93.3	~40	0.69	*Nat. Commun.*, ***2022**, 13, 1129.*
NiRu ball-flower	500 mM NO_3^- + 1000 mM KOH	93.6	~280	~1.95	*Angew. Chem. Int. Ed.*, ***2023**, 62, e202305695.*
$Cu_{50}Ni_{50}$	100 mM NO_3^- + 1000 mM KOH	99	~170	/	*J. Am. Chem. Soc.*, ***2020**, 142, 5702-5708.*
Cu nanowire	500 ppm NO_3^- + 100 mM KOH	96.5	~40	~0.18	*Angew. Chem. Int. Ed.*, ***2023**, 62, e2022218717.*
$Ru_{15}Co_{85}$ HNDs	100 mM NO_3^- + 100 mM KOH	97	~97	1.23	*Nat. Catal*, ***2023**, 6, 402-414.*

References

[1] Y. F. Shen, R. P. Zerger, R. N. Deguzman, S. L. Suib, L. McCurdy, D. I. Potter, C. L. O'Young, Science, 1993, 260, 511–515.

[2] B. Ravel and M. Newville, J. Synchrotron Rad., 2005, 12, 537-541.

[3] S. I. Zabinsky, J. J. Rehr, A. Ankudinov, R. C. Albers, M. J. Eller, Phys. Rev. B, 1995, 52, 2995−3009.

[4] B. Delley, The Journal of Chemical Physics, 2000, 113, 7756-7764.

[5] J. P. Perdew, K. Burke and M. Ernzerhof, Physical Review Letters, 1996, 77, 3865-3868.

[6] A. Klamt, V. Jonas, T. Bürger and J. C. W. Lohrenz, The Journal of Physical Chemistry A, 1998, 102, 5074-5085.

[7] B. Delley, Physical Review B, 2002, 66, 155125.

[8] J. K. Nørskov, J. Rossmeisl, A. Logadottir, L. Lindqvist, J. R. Kitchin, T. Bligaard and H. Jónsson, The Journal of Physical Chemistry B, 2004, 108, 17886-17892.

[9] A. A. Peterson, F. Abild-Pedersen, F. Studt, J. Rossmeisl and J. K. Nørskov, Energy & Environmental Science, 2010, 3, 1311-1315.

[10] W. Luo, W. Xie, R. Mutschler, E. Oveisi, G. L. De Gregorio, R. Buonsanti and A. Züttel, ACS Catalysis, 2018, 8, 6571-6581.

[11] W. Ma, S. Xie, X.-G. Zhang, F. Sun, J. Kang, Z. Jiang, Q. Zhang, D.-Y. Wu and Y. Wang, Nature Communications, 2019, 10, 892.

[12] D. Zhu, L. Zhang, R. E. Ruther, R. J. Hamers, Nat. Mater. 2013, 12, 836-41.

[13] L. C. Green, D. A. Wagner, J. Glogowski, P. L. Skipper, J. S. Wishnok, S. R. Tannenbaum, Anal. Biochem. 1982, 126, 131-138.

[14] G. W. Watt and J. D. Chrisp, Anal. Chem., 1952, 24, 20062008.